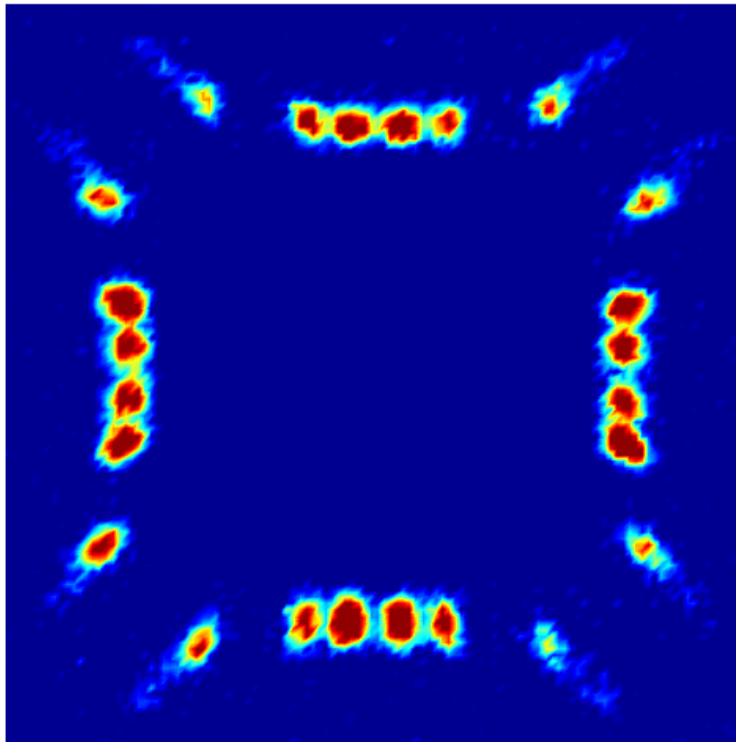


# Flux line lattice forays using SANS



2008 Summer School on Small Angle Neutron Scattering

NIST Centre for Neutron Research

The flux line lattice (**FLL**) of Type-II superconductors is a topic of much recent interest. The FLL may be imaged directly using small-angle neutron scattering (**SANS**). Since subtle properties of the underlying superconducting state may be reflected in the orientation and shape of the FLL, and in the flux line form factor, SANS studies of the FLL continue to both challenge and propel our understanding of superconductivity.

The objectives of this experiment are to develop a cursory comprehension of what FLL studies entail. Without being too caught in the specifics, it is also hoped the participant will attain a familiarity with the diffraction technique, essential for SANS studies of the FLL, but moreover very useful for neutron or X-ray explorations of other systems.

We will first begin with an outline of superconductivity, describing fundamental theories and features that must be borne in mind throughout any FLL study. In section 2 we turn our attention to diffraction theory at a level appropriate for our introductory FLL experiment. With the aim of providing a handy reference for the reader, with the relevant ideas collected in one place, this second section takes rather a formal approach. The SANS instrument and associated considerations are outlined in section 3. Finally in 4 the details are given of the superconductor (niobium) chosen for our introductory experiment, and a list of several research topics is proposed, any one of which can be readily investigated in the pedagogical beamtime available. Throughout this treatise, questions may be discovered, to stimulate the conscious reader.

## 1 Superconductivity

It is nearly a century since superconductivity was discovered in 1911 by Kamerlingh-Onnes who observed an abrupt drop to zero of the resistivity of mercury below  $T_c \approx 4\text{K}$ . It is just twenty or so years since the *high- $T_c$*  superconductors were discovered: in 1986 by Bednorz and Müller [1] in the La-Ba-cuprate system ( $T_c \approx 36\text{K}$ ) and in the following year by Wu *et al.* [2] in the Y-Ba-cuprate (YBCO) system with a  $T_c \approx 93\text{K}$ . This temperature is accessible using liquid nitrogen, making YBCO today's superconducting star of laboratory demonstrations.

Under the influence of an applied magnetic field, mercury has quite different superconducting properties from the cuprates. Hg will expel from its bulk *all* applied field below  $H_c(T)$  in an effect commonly accredited to Meißner, rather neglecting his postdoctoral collaborator Ochsenfeld, following their discovery in 1933. In the cuprates the perfect diamagnetism holds only below a lower critical field  $H_{c1}(T)$ . Above this *Meissner phase*, but below the

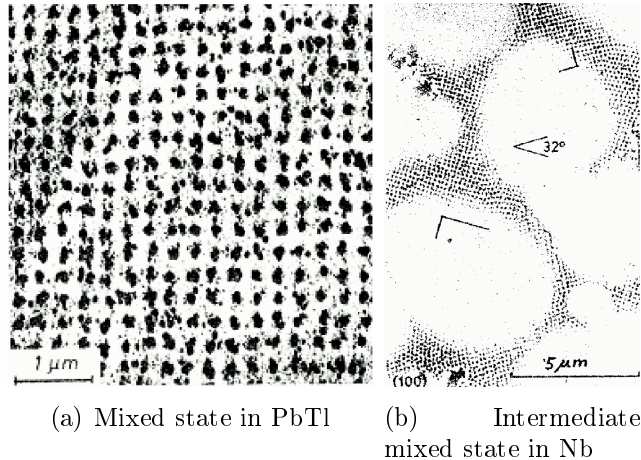


Figure 1: Pictures produced by Bitter decoration — where ferromagnetic nanoparticles are absorbed onto the surface of a superconductor — with field applied parallel to the crystal  $\langle 100 \rangle$  direction, from Obst [3].

normal-superconducting transition at an upper critical field  $H_{c2}(T)$ , the field penetrates as *lines* of magnetic flux with each flux line carrying one quantum of flux  $\Phi_0 \equiv \frac{h}{2e}$ . Superconductors that exhibit this *mixed state* (Fig. 1(a)) are designated as ‘Type-II’, whereas those like Hg are ‘Type-I’.

The interaction between flux lines is usually repulsive at all spacings, though for certain superconductors (such as high-purity niobium) a long-range attractive FL interaction just above  $H_{c1}(T)$  may (depending on the sample shape) result in an *intermediate mixed state* composed of Meissner regions and regions of constant flux density  $B_0$  (Fig. 1(b)).

*Q. Are the values of “induction” and “flux density” different in the mixed state? What about in the intermediate mixed state?*

In Fig. 2 we plot the phase diagram typical of a Type-II superconductor possessing an intermediate mixed state.

## 1.1 Phenomenological Theories

At zero field, the normal to superconducting transition is second order i.e. the order parameter describing the superconductivity goes continuously to zero as  $T \rightarrow T_c$ . Thus, following the usual approach of Ginzburg and Landau, the free energy may be expanded in powers of the order parameter. In his Nobel prize-winning work, Abrikosov showed that the lowest energy solution of the Ginzburg-Landau equations for fields  $H_{c1} < H < H_{c2}$  is indeed a lattice of

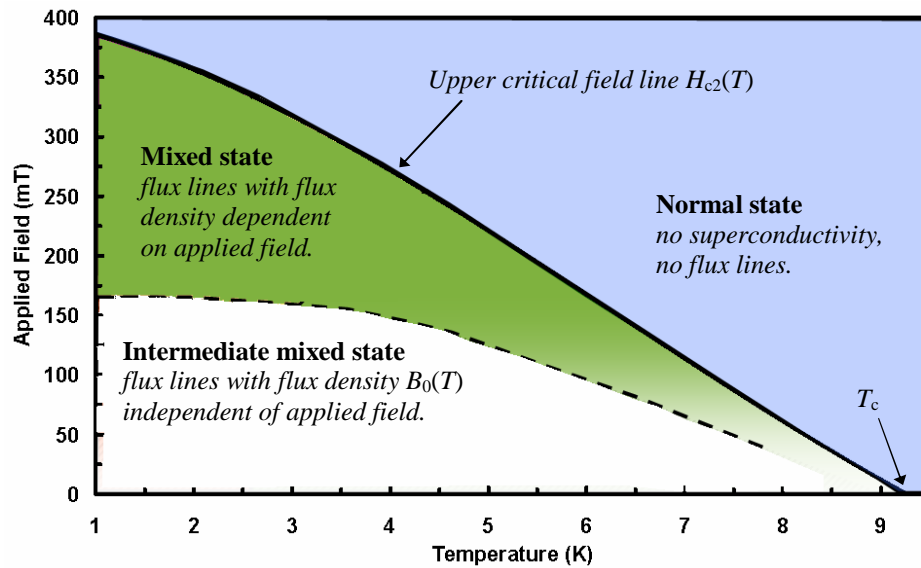


Figure 2: Diagram depicting the different states present in high-purity niobium, as a function of temperature and field applied parallel to the fourfold [001] crystal axis. The upper critical field  $H_{c2}(T)$  is independent of sample shape, since at these fields the sample magnetization is zero. However the *applied* field below which the intermediate mixed state is entered depends on the sample shape via a demagnetization factor; here this line is representative of a *cylindrical* sample.

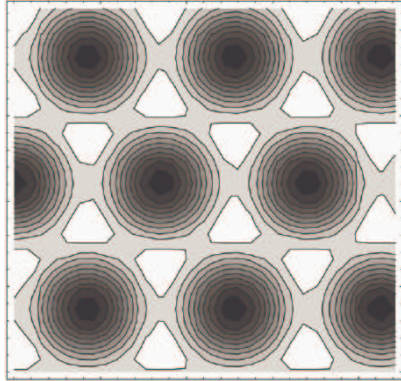


Figure 3: The order parameter of the Abrikosov solution to the Ginzburg-Landau equations, solved in the lowest Landau level approximation.

flux lines [4], with the area  $A$  of one FLL unit cell satisfying the condition

$$\Phi_0 = BA \quad (1)$$

where  $B$  is the *flux density* and  $\Phi_0 \equiv \frac{h}{2e} = 2.07 \times 10^{-15} \text{ Tm}^2$  is the flux quantum.

**Q.** *How does  $A$  change as a function of applied field  $H$  for high-purity Nb (c.f. Fig. 2) ?*

Abrikosov further showed that the Ginzburg-Landau free energy is sensitive to the shape of the FLL, with the free energy density a monotonically increasing function of the geometrical parameter  $\beta_A$ . In the simplest — i.e. isotropic — case, a square FLL coordination has  $\beta_A = 1.18$  while a hexagonal coordination yields  $\beta_A = 1.16$ . Thus the equilibrium FLL prefers an equilateral triangular half-unit cell in the isotropic situation (Fig. 3). It is easy to envisage that underlying anisotropies of the superconductor can manifest themselves as equilibrium distortions from the equilateral triangle, or as transitions into other FLL structures. In the high- $T_c$  cuprate superconductors (such as YBCO), for example, a square FLL at high fields is believed to stem from an asymmetric  $d$ -wave order parameter.

**Q.** *Can you guess what FLL structures may give rise to the 2D diffraction image on the cover of this treatise ?*

In Fig. 4 the structure of an isolated flux line is illustrated. The core of each flux line is *not* superconducting — it is in the normal state. The diagram illustrates the important parameters in superconductivity:

- the Ginzburg-Landau coherence length  $\xi$  measures the distance over which the superconducting order parameter responds to a perturbation;
- the London penetration depth  $\lambda_L$  is the characteristic length of the decay of any field from a normal region, in this case the core of a flux line;

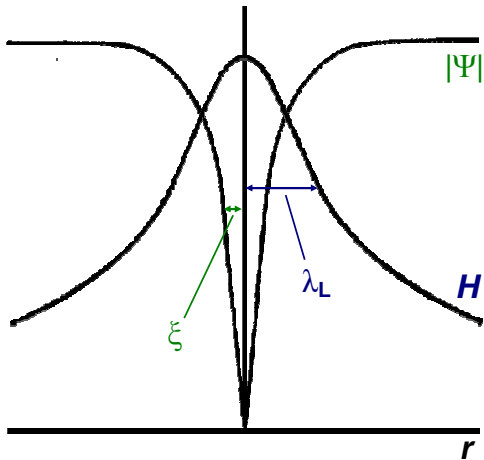


Figure 4: Structure of an isolated flux line in a Type-II superconductor calculated using Ginzburg-Landau theory with  $\kappa = 20$ . Going outwards, the magnetic field  $H$  decreases with the penetration depth  $\lambda_L$ , while the order parameter  $\Psi$  is reduced in a core region of radius  $\xi$ .

- the Ginzburg-Landau parameter  $\kappa$  which is, roughly, the ratio  $\lambda/\xi$ .

The Ginzburg-Landau theory is only strictly valid in the region where the order parameter becomes vanishingly small i.e. at temperatures close to  $T_c$ . In 1935, some score years before the prime of Landau and Ginzburg, the brothers F. and H. London proposed a phenomenological description of the superconducting state in the limit where all magnetic fields and supercurrents are weak and have a slow variation in space. In this description, a densely packed array of flux lines is represented by two-dimensional delta functions in the London equation

$$\mathbf{H} + \lambda_L^2 \nabla \wedge \nabla \wedge \mathbf{H} = \Phi_0 \hat{\mathbf{z}} \sum_j \delta(\mathbf{r}^\perp - \mathbf{R}_j^\perp) \quad (2)$$

where the flux lines are directed along the  $z$ -axis and  $\mathbf{R}_j^\perp$  is the position of the  $j$ th flux line in the  $(x, y)$  plane.

It is easy to see that, if just one flux line is considered in (2), that the field decays exponentially away from the core with characteristic length  $\lambda_L$ . In (2) one assumes that the core of each flux line has a vanishingly small radius  $\xi \rightarrow 0$  so that the corresponding singularity can be replaced by a delta function, and that the contributions from isolated flux lines can be simply superimposed. These assumptions are acceptable if  $\xi \ll d \ll \lambda_L$  where  $d$  is the spacing between flux lines. We will return to (2) in regard of the flux line *form factor*, a quantity measurable using SANS.

## 2 Bragg diffraction

We start with the elastic differential cross-section giving the probability of neutrons scattering into a solid angle  $d\Omega$

$$\frac{d\sigma}{d\Omega} = \left(\frac{m_n}{2\pi\hbar^2}\right)^2 \left| \int \hat{V}(\mathbf{r}) e^{i\boldsymbol{\kappa}\cdot\mathbf{r}} d\mathbf{r} \sum_j^N e^{i\boldsymbol{\kappa}\cdot\mathbf{R}_j} \right|^2 \quad (3)$$

where  $m_n$  is the neutron mass,  $\hat{V}$  is the *Fermi pseudo-potential* that is defined (in the *Born approximation*) to give isotropic scattering from one of the  $N$  similar scatterers centred at  $\mathbf{R}_j$ .  $\boldsymbol{\kappa}$  is known as the *scattering vector*. These italicised terms and (3) *should* already be familiar from the opening lectures of this summer school. For the basic concepts of neutron scattering set in a wider context, the keen reader is referred to Squires [5] and Lovesey [6].

We see that (3) separates into a *structure factor*

$$S(\boldsymbol{\kappa}) \equiv \left| \sum_j^N e^{i\boldsymbol{\kappa}\cdot\mathbf{R}_j} \right|^2 \quad (4)$$

and a *form factor*  $F_A(\boldsymbol{\kappa})$  that is simply the Fourier transform of the potential for a single scatterer

$$F_A(\boldsymbol{\kappa}) \equiv \frac{m_n}{2\pi\hbar^2} \int \hat{V}(\mathbf{r}) e^{i\boldsymbol{\kappa}\cdot\mathbf{r}} d\mathbf{r} \quad (5)$$

### 2.1 An array of flux lines

The magnetic moment operator for a neutron is  $\boldsymbol{\mu} = -\gamma\mu_N\boldsymbol{\sigma}$  where  $\boldsymbol{\sigma}$  is the Pauli spin operator, the nuclear magneton  $\mu_N \equiv \frac{e\hbar}{2m_p}$  and the neutron gyromagnetic ratio  $\gamma = 1.913$ . The interaction of a neutron with a magnetic field  $\mathbf{H}$  is described by the potential

$$-\boldsymbol{\mu}\cdot\mathbf{H} = -\gamma\mu_N\boldsymbol{\sigma}\cdot\mathbf{H}$$

The operator  $\boldsymbol{\sigma}$  depends on the spin coordinates of the neutron. With *unpolarised* incident neutrons,  $H = |\mathbf{H}|$ , and the elastic differential cross-section (3) becomes

$$\begin{aligned} \frac{d\sigma}{d\Omega} &= \left(\frac{m_n}{2\pi\hbar^2}\right)^2 \gamma^2 \mu_N^2 \left| \int H(\mathbf{r}) e^{i\boldsymbol{\kappa}\cdot\mathbf{r}} d\mathbf{r} \right|^2 S(\boldsymbol{\kappa}) \\ &= \frac{\gamma^2}{16\Phi_0^2} \left| \int H(\mathbf{r}) e^{i\boldsymbol{\kappa}\cdot\mathbf{r}} d\mathbf{r} \right|^2 S(\boldsymbol{\kappa}) \end{aligned}$$

since  $\mu_N \simeq \frac{e\hbar}{2m_n}$  and the flux quantum  $\Phi_0 \equiv \frac{h}{2e}$ .

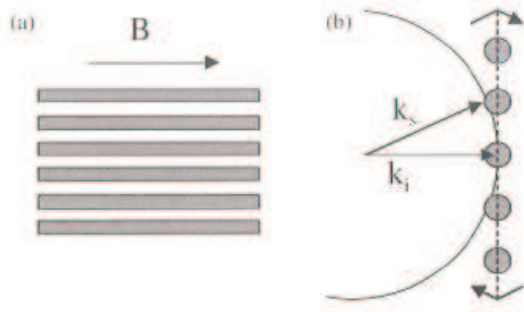


Figure 5: A perfect flux line lattice is shown in (a) viewed perpendicular to the field direction. The cores of the flux lines are shaded. The periodic field distribution leads to a two-dimensional array of spots in reciprocal space (b). These are swept through the Ewald sphere (that defines the locus of points where the scattering is elastic) as the FLL is rotated. Reproduced from Huxley [7].

## 2.2 A perfect flux line lattice

Here we consider the flux line lattice (FLL) as a regular arrangement of rigid straight rods. The perfect arrangement in real space leads to a 2D array of spots in reciprocal space (Fig. 5). For a large (infinite) crystal the structure factor (4) exhibits  $\delta$ -function peaks in the usual way

$$S(\boldsymbol{\kappa}) \propto \delta(\boldsymbol{\kappa} - \mathbf{G})$$

$\mathbf{G}$  is a reciprocal lattice vector of the FLL. We observe no elastic scattering unless the Bragg condition  $\boldsymbol{\kappa} = \mathbf{G}$  and the elastic condition  $|\mathbf{k}| = |\mathbf{k}'|$  are satisfied, where  $\mathbf{k}$  and  $\mathbf{k}'$  are the incident and scattered wave vectors respectively (note  $\boldsymbol{\kappa} \equiv \mathbf{k} - \mathbf{k}'$ ). These relations are combined in a more familiar form of Bragg's law

$$2d \sin \theta_B = n \lambda_n$$

where  $n \in \mathbb{Z}$ ,  $d$  is the Bragg plane spacing,  $2\theta_B$  is the angle between incident  $\mathbf{k}$  and diffracted  $\mathbf{k}'$  neutrons, and  $\lambda_n$  is the neutron wavelength. For typical flux line spacings  $d \approx 1000 \text{ \AA}$  (*Q. To what flux density would this correspond? c.f. (1)*), and employing cold neutrons ( $\lambda_n \approx 10 \text{ \AA}$ ), we find  $\theta_B \approx 0.3^\circ$ , perhaps not surprisingly favouring the use of a SANS instrument.

## 2.3 The rocking curve

By rotating the sample (and cryomagnet) through a Bragg peak (the “rocking curve”) we collect an integrated intensity  $I_{\mathbf{G}}$  that, when normalised to the

incident neutron flux  $I_0$ , yields an integrated reflectivity

$$R_{\mathbf{G}} \equiv \frac{I_{\mathbf{G}}}{I_0} = \frac{\gamma^2}{16} \frac{\lambda_n^3}{A^2 \sin 2\theta_B} t |h_{\mathbf{G}}|^2 \quad (6)$$

where  $t$  is the illuminated sample thickness and  $A$  is the FLL unit cell area. The form factor  $h_{\mathbf{G}}$  is defined as the normalized Fourier transform of the two-dimensional field distribution for a single flux line

$$h_{\mathbf{G}} = \frac{\int H(\mathbf{r}) e^{i\mathbf{G}\cdot\mathbf{r}} d\mathbf{r}}{\Phi_0} \quad (7)$$

where  $\Phi_0$  is the flux quantum.

**Q.** *What is the field dependence of  $h_{\mathbf{G}}$  as predicted by the London equation (2) ?*

The integrated reflectivity (6) is particularly useful as it can be measured in absolute units and is independent of the instrument resolution function and any small mosaic spread arising from more than one FLL crystallite existing in different regions of the sample.

Although not as pleasing to the eye as FLL structural studies, the flux line form factor may be of great consequence as demonstrated in very recent work [8] where an anomalous field dependence of the form factor *may* indicate the presence of a novel, inhomogeneous superconducting state known as the Fulde-Ferrell-Larkin-Ovchinnikov state.

### 3 SANS instruments

A schematic of the general SANS instrument is shown in Fig. 6. At the NCNR, the two 30 m SANS instruments (NG3-SANS and NG7-SANS) allow a neutron wavelength in the range 5–20 Å, determined by the rotational speed of the velocity selector. The wavelength spread can also be changed by tilting the velocity selector axis with respect to the beam direction, though  $\approx 15\%$  is typically used. For FLL studies, usually a small angular spread is affected by removing all 8 of the neutron guides. With this maximum collimation, we also have a choice of source apertures (placed upstream of the collimation), namely 1.43 cm, 2.20 cm or 3.81 cm. Due to the small Bragg angles involved, the detector is usually placed as far downstream as possible.

The simple geometry of a SANS experiment (Fig. 7) means that the instrument resolution function can easily be calculated. Some insight can be derived into the instrument resolution, and moreover the long range structure and degree of order of the FLL, by using a mathematically convenient model in which contributions to the finite width of observed diffraction spots

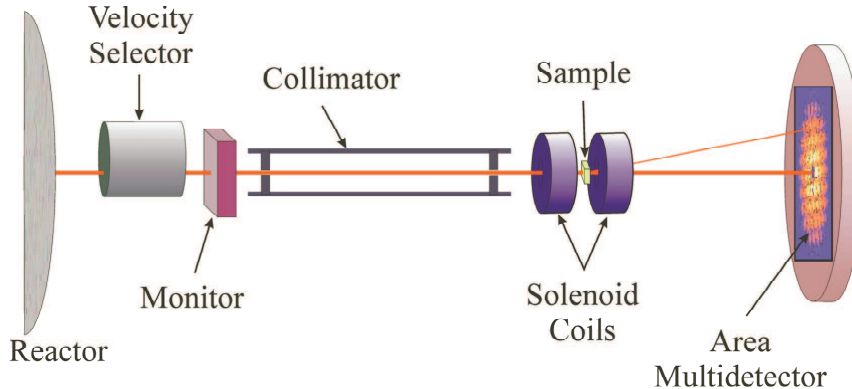


Figure 6: A schematic of a typical SANS instrument. An incoming neutron beam with wavelength spread  $\approx 15\%$  and small angular spread  $\approx 0.1^\circ$  is prepared by a velocity selector and a collimation of up to 15 m. A similar distance between the sample and the multidetector allows the detection of neutrons scattered at small angles.

are represented by Gaussians with similar standard deviations to the actual distributions [9]. These contributions include the angular spread  $a$  of the incoming beam  $\mathbf{k}_i$ , the effective spread  $b$  of the Bragg plane *angle* away from the mean — in reciprocal space this is the angular spread of  $\boldsymbol{\kappa}$  in the scattering plane; the effective spread  $c$  of the Bragg angle  $\theta_B$  i.e. the spread in the magnitude of the scattering vector  $|\boldsymbol{\kappa}|$ .

The angular spread of the incoming beam is determined by the collimation and a pair of apertures at either end. The *source* aperture denotes the aperture closest to the neutron source, while the defining or *sample* aperture is closest to the sample. Here we considering the source and sample apertures as thin slits of width  $s_o$  and  $s_a$  respectively. The FWHM  $a$  is [10]

$$a \simeq \begin{cases} \frac{s_o}{l_c}, & \frac{s_o}{l_c + l_d} \geq \frac{s_a}{l_d} \\ s_a \left( \frac{1}{l_c} + \frac{1}{l_d} \right), & \text{otherwise} \end{cases} \quad (8)$$

Here  $l_c$  is the collimating distance between the apertures and  $l_d$  is the distance from the sample aperture to the detector. For circular apertures a more complicated geometrical construction contributes small corrections to (8) [10].

With the geometry of Fig. 7,  $b$  is a measure of the correlations *along* the flux lines that give a finite width  $W_L$  of the spot in reciprocal space parallel to the field.  $b$  will in addition include any small mosaic spread that contributes to a resolvable Bragg peak.

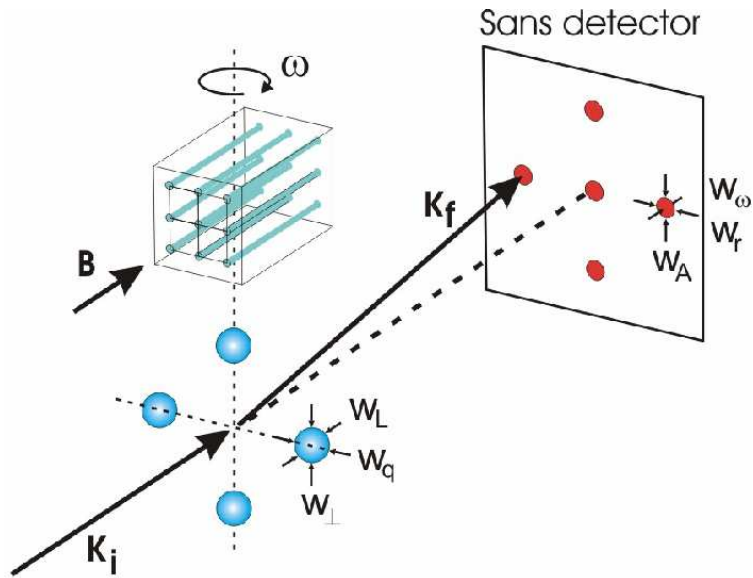


Figure 7: The experiment geometry usually chosen for FLL SANS experiments. A square FLL is illustrated in real and reciprocal space. *Q.* How are the 2D real and reciprocal space lattices related for a FLL of arbitrary shape? Measurement of the angular width of the rocking curves  $W_\omega$  and the radial  $W_r$  and azimuthal  $W_A$  widths of a diffraction spot projected on the detector allows estimation of the size of the spot in reciprocal space in three dimensions; this may be expressed by variation  $W_q$  in the length of the reciprocal vector  $G$  and widths of the spot in reciprocal space parallel  $W_L$  and perpendicular  $W_\perp$  to the field.

The wavelength spread  $\Delta\lambda_n/\lambda_n$  of the incoming beam plus the spread  $W_q = \Delta G/G$  in spacing between FLL Bragg planes are combined in  $c$

$$\left(\frac{c}{\theta_B}\right)^2 = \left(\frac{\Delta\lambda_n}{\lambda_n}\right)^2 + W_q^2 \quad (9)$$

Here we will focus on the rocking curve width  $W_\omega$ . By integrating over the distribution in diffracted beam as a function of rocking angle  $\omega$ , one finds

$$W_\omega^2 = a^2 + b^2 + c^2 \quad (10)$$

For small angle scattering we see from (9) the spread  $c$  in Bragg angle is small, even for the  $\approx 15\%$  wavelength spread coming from a velocity selector. This makes the typical SANS instrument employing a velocity selector quite *insensitive* to  $W_q$ . For the rocking curve width (10) the instrument resolution is essentially the angular spread of the incoming beam — typically  $\approx 0.1^\circ$ .

## 4 Introductory experiment

For our pedagogical experiment, the FLL in high-purity elemental niobium will be examined. Nb has the following superconducting parameters:

- $T_c = 9.3$  K
- $\kappa = 0.7$
- $\xi_0 = 390$  Å

**Q.** *For what field region, if any, is the London theory valid for this low- $\kappa$  superconductor?*

Our sample will be a single-crystal Nb sphere of diameter  $\approx 13$  mm, mounted on a closed-cycle refrigerator with a base temperature of 1.9 K. The refrigerator and sample will be inserted into an electromagnet, providing fields of up to 500 mT applied parallel to the fourfold [001] axis of the body-centred cubic niobium. The  $(H, T)$  phase diagram for this situation is illustrated in Fig. 2. The FLL should be formed by applying the field at a temperature above  $T_c$  before cooling in the field. The sample, electromagnet and CCR are fixed onto a rotation stage which, by suitable scans of the rotation angle, enables rocking curves to be measured. Data analysis will be carried out using the Grasp package, illustrated in Fig. 8 to aid pre-experiment familiarity. Detailed help on this analysis package will be available at the instrument.

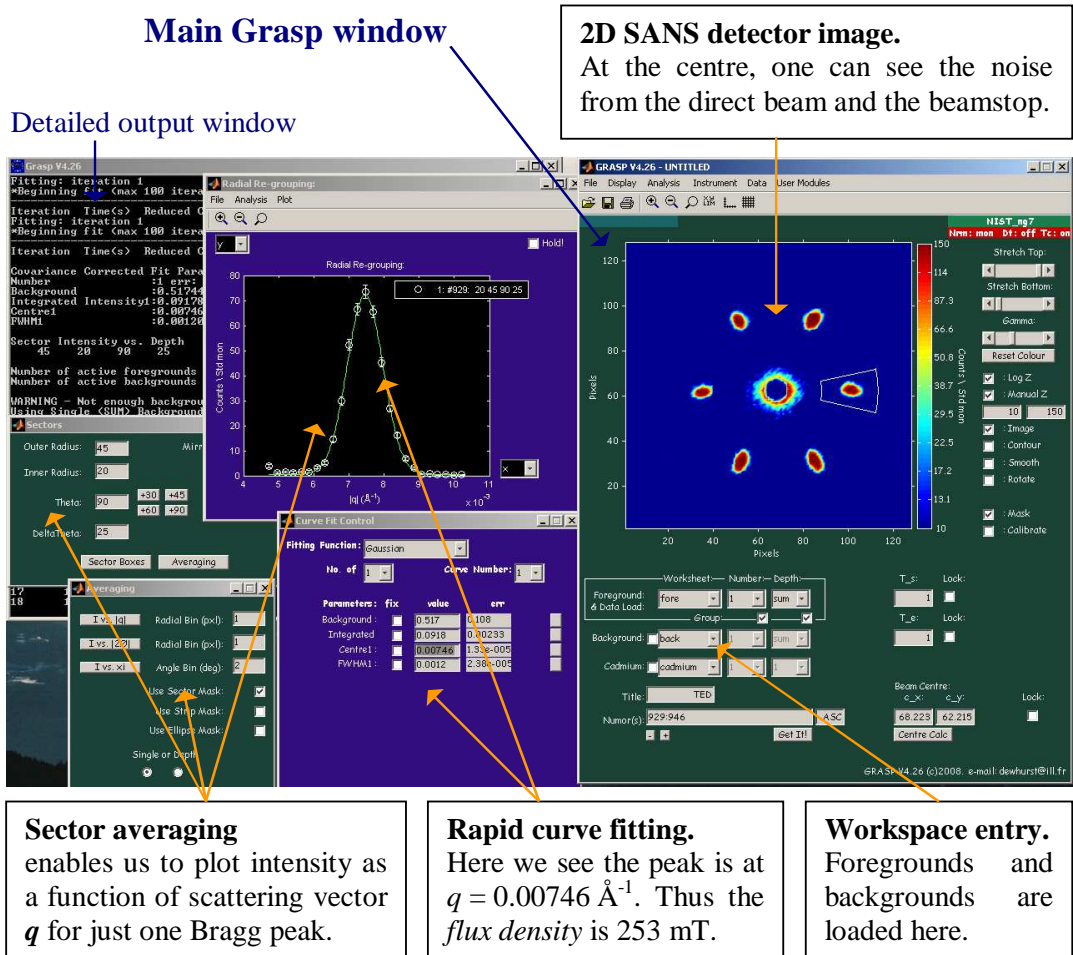


Figure 8: A typical example of the use of Grasp. Here the flux density of a hexagonal FLL is measured.

Our treatise is concluded with a list of suggested topics, any one of which (or more for the very keen) is suitable for the short summer-school study. They are:

- An investigation of FLL structure as a function of applied field in both the mixed state and intermediate mixed state at base temperature (1.9 K).
- An investigation of FLL structure as a function of temperature at an applied field of either i) 175 mT (in the mixed state), ii) 100 mT (concentrating on the intermediate mixed state), iii) low applied fields close to  $T_c$ .
- An investigation of the temperature dependence of  $B_0$ , carried out at a suitable applied field (c.f. Fig. 2).
- A precise determination of the applied field at which the intermediate mixed state is entered for our spherical sample at some suitable temperature (note Fig. 2 is representative of a cylindrical sample).
- An exploration of the flux line form factor as a function of applied field in the mixed state at base temperature.
- An exploration of the flux line form factor as a function of temperature in the mixed state at an applied field of 175 mT.

It is left to each summer-school group to choose and direct their study, but your friendly instrument scientist will, as always, be on hand — so have fun !!

## References

- [1] J. G. Bednorz and K. A. Müller, *Z. Phys. B* **64**, 189 (1986).
- [2] M. K. Wu, J. R. Ashburn, C. J. Torng, P. H. Hor, R. L. Meng, L. Gao, Z. J. Huang, Y. Q. Wang, and C. W. Chu, *Phys. Rev. Lett.* **58**, 908 (1987).
- [3] B. Obst, in *Anisotropy effects in superconductors*, edited by H. W. Weber (Plenum, New York, 1977), p. 139.
- [4] A. A. Abrikosov, *Sov. Phys. JETP* **5**, 1174 (1957).

- [5] G. L. Squires, *Intoduction to the theory of thermal neutron scattering* (Cambridge University Press, Cambridge, 1978).
- [6] S. W. Lovesey, *Theory of neutron scattering from condensed matter* (Oxford University Press, Oxford, 1984), Vol. 1.
- [7] A. Huxley, in *Vortices in unconventional superconductors and superfluids*, edited by R. P. Huebener, N. Schopohl, and G. E. Volovik (Springer-Verlag, Berlin, 2002), pp. 301–339.
- [8] A. D. Bianchi, M. Kenzelmann, L. DeBeer-Schmitt, J. S. White, E. M. Forgan, J. Mesot, M. Zolliker, J. Kohlbrecher, R. Movshovich, E. D. Bauer, J. L. Sarrao, Z. Fisk, C. Petrović, and M. R. Eskildsen, *Science* **319**, 177 (2008).
- [9] R. Cubitt, E. M. Forgan, D. McK. Paul, S. L. Lee, J. S. Abell, H. Mook, and P. A. Timmins, *Physica B* **180**, 377 (1992).
- [10] J. S. Pedersen, D. Posselt, and K. Mortensen, *J. Appl. Cryst.* **23**, 321 (1990).